Phase diagram for a topological Kondo insulating system

Minh-Tien Tran,[1,2] Tetsuya Takimoto,[1,3] and Ki-Seok Kim[1,3]

[1]*Asia Pacific Center for Theoretical Physics, POSTECH, Pohang, Gyeongbuk 790-784, Republic of Korea*

[2]*Institute of Physics, Vietnamese Academy of Science and Technology, P.O. Box 429, 10000 Hanoi, Vietnam*

[3]*Department of Physics, POSTECH, Pohang, Gyeongbuk 790-784, Republic of Korea*

(Received 27 September 2011; revised manuscript received 11 February 2012; published 26 March 2012)

The discovery of topological insulators in noninteracting electron systems has motivated the community to research such topological states of matter in correlated electrons both theoretically and experimentally. In this paper, we investigate a phase diagram for a topological Kondo insulating system, where an emergent "spin'-dependent Kondo effect gives rise to an inversion for heavy-fermion bands, responsible for a topological Kondo insulator. Using U(1) slave-boson mean-field analysis, we uncover an additional phase transition inside the Kondo insulating state in two dimensions, which results from the appearance of the topological Kondo insulator. On the other hand, we observe that the Kondo insulating state can be separated into three insulating phases in three dimensions, identified as the weak topological Kondo insulator, the strong topological Kondo insulator, and the normal Kondo insulator, respectively, and classified by Z_2 topological indices. We discuss the possibility of novel quantum criticality between the fractionalized Fermi liquid and the topological Kondo insulator, where the band inversion occurs with the formation of the heavy-fermion band at the same time.

DOI: 10.1103/PhysRevB.85.125128 PACS number(s): 71.10.Hf, 71.27.+a

I. INTRODUCTION

An effective field theory approach has been playing an important role in predicting novel quantum states of matter. Essential physical contents in the field theory approach are the chiral anomaly for quantum number fractionalization,[1] the parity anomaly for the quantum Hall effect,[2] and an SU(2) global anomaly[3] for topological insulators in three dimensions.[4] However, the field theory approach alone is not sufficient to thoroughly research such quantum matter in real materials. It is necessary to construct or find the corresponding lattice model, which can result in an ideal effective field theory at low energies. In particular, the lattice model can be solved almost exactly based on numerical simulations, helping us to understand the connection between the lattice model and effective field theory and verifying the possibility of novel quantum phenomena.

The Su-Schrieffer-Heeger model, which describes one-dimensional electrons coupled with lattices, confirms the existence of $e/2$ fractional electric charge, carried by domain-wall solitons.[5] The Haldane model, which describes two-dimensional electrons with a next-nearest-neighbor complex hopping parameter on the honeycomb lattice, explains the integer quantum Hall effect without Landau levels,[6] where each Dirac band carries a nontrivial topological quantum number (Chern number), identified with the quantized Hall conductance.[7] Recently, the Haldane model has been generalized to the case with time-reversal invariance, where the spin-orbit coupling serves as an effective magnetic flux, oppositely assigned to spin-up and -down electrons, thus regarded as two duplicates of the Haldane model. The Kane-Mele model has proposed an interesting insulating state, called a topological insulator, where the quantum spin Hall effect appears when the z component of the spin quantum number is preserved, but generically classified by the Z_2 topological quantum number with spin-non-conserving terms.[8] The concept of the topological insulator was extended to the three-dimensional case,[9–11] characterized by the Z_2 topological index, which counts the number of band inversions with modular 2. An odd number of band inversions causes an odd number of Dirac bands, identified with normalizable fermion zero modes localized at each two-dimensional surface, where at least one of them is protected against time-reversal-invariant perturbations due to a topological origin.

Considering that these models basically describe non-interacting electrons, an immediate and important question concerns the role of electron correlations in such topological states of matter.[12] Actually, this direction of research has been performed intensively, focusing in particular on the emergence of gapped spin liquids,[13] where spinons with fractional spin quantum number $1/2$ appear as elementary excitations. The quantum dimer model on the triangular lattice has confirmed the existence of a short-ranged resonating valence bond state, identified with Z_2 spin liquid.[14] It has been claimed that this gapped spin liquid state has appeared in strongly correlated electrons on the honeycomb lattice.[15] Such an effect has also been realized in strongly correlated spinless fermions,[16] which allow charge fractionalization in geometrically frustrated lattices. Artificial but exactly solvable spin models, represented as the Kitaev model,[17] have been investigated, proving the existence of topologically nontrivial quantum states of matter, for example a non-Abelian quantum Hall state, which allows Majorana fermions.[18] Such exotica have also been pursued near quantum criticality, referred to as deconfined quantum criticality, where an effective field theory approach had suggested the emergence of spin quantum number fractionalization at an antiferromagnet to valence-bond solid quantum critical point,[19] and numerical simulations for an extended Heisenberg model on the square lattice confirmed this scenario with some modifications.[20,21]

Recently, it has been argued that the fractional quantum Hall effect appears in a certain type of lattice models, whose characteristic feature is the existence of an almost flat band with a nontrivial Chern number.[22] Electron correlations for this partially filled flat band with the Chern number were demonstrated to result in the fractional quantum Hall phase.

An immediate and interesting question is how to construct the lattice model, which shows the so-called fractional topological insulator. An effective field theory approach suggested the possibility of the fractional topological insulator,[23,24] characterized by the fact that the surface Dirac fermion carries a fractional electric charge, which should be distinguished from the fractionalized "normal' insulator, not allowing gapless surface modes. A hard-core boson model was proposed on the diamond lattice, where the boson is assumed to fractionalize into two fermions with $e/2$ fractional charge, forming a topological band insulator for such fractionalized fermions and displaying the fractional magnetoelectric effect.[25] Introducing electron correlations into the Kane-Mele model,[26,27] an interesting spin liquid state was proposed to exhibit an integer quantum spin Hall effect in the case of S_z conservation.

In this paper, we construct an elementary setup for the possible interplay between electron correlations and topological aspects in the presence of time-reversal symmetry. Recently, a topological Kondo insulating state has been proposed to open a novel direction of research for interacting topological states of matter.[28] The existence of the topological Kondo insulator is based on an emergent "spin'-dependent Kondo effect, which plays basically the same role as the spin-orbit interaction and gives rise to an inversion for heavy-fermion bands. We revisit this problem, investigating an effective Anderson lattice model for the topological Kondo insulator, where this effective Hamiltonian can be regarded as one of the most studied models, particulary for non-Fermi-liquid physics near heavy-fermion quantum criticality.[29]

Using U(1) slave-boson mean-field analysis, we uncover an additional phase transition inside the Kondo insulating state in two dimensions, which results from the appearance of the topological Kondo insulator. On the other hand, we observe that the Kondo insulating state can be separated into three insulating phases in three dimensions, identified as the weak topological Kondo insulator, the strong topological Kondo insulator, and the normal Kondo insulator, respectively, and classified by Z_2 topological indices. Such phase transitions inside the Kondo insulator are described by gap closing, which is expected to be continuous. We derive an effective Dirac theory near the gap closing momentum point for the phase transition from the strong topological Kondo insulator to the normal Kondo insulator.

We would like to emphasize that the phase diagram of the present study differs from that of the previous investigation[28] in that our phase diagram is constructed in the plane of the hybridization coupling and temperature, while the previous phase diagram displays a phase structure as a function of an effective orbital energy for localized electrons at zero temperature. However, the mechanism for the emergence of the topological Kondo insulator is essentially the same.

II. PHASE DIAGRAM FOR A TOPOLOGICAL KONDO INSULATOR

A. An effective Anderson lattice model

In order to consider the topological nature of the heavy-electron system, we construct the simplest model, which introduces one s orbital and one f orbital in the unit cell. Conduction electrons are described by

$$H_c = \sum_{\boldsymbol{k}} \sum_{\sigma} \left(\varepsilon^c_{\boldsymbol{k}} - \mu_c\right) c^\dagger_{\boldsymbol{k}\sigma} c_{\boldsymbol{k}\sigma}, \tag{1}$$

where $\varepsilon^c_{\boldsymbol{k}}$ is the dispersion relation of the conduction electron with momentum $\boldsymbol{k}$ and real spin σ, and μ_c is the electron chemical potential. The f-electron Hamiltonian is given by the site energy $\epsilon_f - \mu_c$ and the on-site Coulomb interaction U,

$$H_f = \sum_{\boldsymbol{i}} \sum_{\tau} (\epsilon_f - \mu_c) f^\dagger_{\boldsymbol{i}\tau} f_{\boldsymbol{i}\tau} + U \sum_{\boldsymbol{i}} n_{f\boldsymbol{i}\tau} n_{f\boldsymbol{i}-\tau}, \tag{2}$$

where $n_{f\boldsymbol{i}\tau} = f^\dagger_{\boldsymbol{i}\tau} f_{\boldsymbol{i}\tau}$ is the density operator of the f electron with pseudospin τ belonging to one representation γ of the $j = 5/2$ multiplet at site $\boldsymbol{i}$. $|\boldsymbol{i} - \tau\rangle$ is the time-reversal partner of $|\boldsymbol{i}\tau\rangle$ in the Kramers doublet. Representations other than the γ representation are assumed to be irrelevant.

An essential point is how these itinerant and localized electrons are coupled, generically given by the hybridization term

$$H_{\rm hyb} = \sum_{\boldsymbol{k}} \sum_{\sigma,\tau} V_{\sigma\tau}(\boldsymbol{k}) c^\dagger_{\boldsymbol{k}\sigma} f_{\boldsymbol{k}\tau} + \text{H.c.}, \tag{3}$$

where $f_{\boldsymbol{k}\tau}$ is the Fourier $\boldsymbol{k}$ component of $f_{\boldsymbol{i}\tau}$. In order to determine the structure of $V_{\sigma\tau}(\boldsymbol{k})$, we have to specify the representation γ of the f electron and its surroundings associated with conduction electron sites. If we restrict the f-electron states to the $j = 5/2$ multiplet, the hopping matrix is described by

$$\begin{aligned}\langle \boldsymbol{i}s\sigma|H_{\rm hyb}|\boldsymbol{j}\gamma\tau\rangle \simeq \langle \boldsymbol{i}s\sigma|H_{\rm hyb}|\boldsymbol{j}\eta\sigma\rangle \langle \boldsymbol{j}\eta\sigma|\boldsymbol{j}m\sigma\rangle \\ \times \left\langle \boldsymbol{j}m\sigma \middle| \boldsymbol{j}\, j = \tfrac{5}{2}\mu \right\rangle \left\langle \boldsymbol{j}\, j = \tfrac{5}{2}\mu \middle| \boldsymbol{j}\gamma\tau \right\rangle,\end{aligned} \tag{4}$$

where η is the representation and basis of the cubic harmonic oscillator, m is the z component of the orbital angular momentum of the f electron, and μ is the z component of the total angular momentum. The approximate equality comes from the ignorance of the $j = 7/2$ multiplet in estimating the matrix element.

Resorting to the table of $\langle \boldsymbol{i}s\sigma|H_{\rm hyb}|\boldsymbol{j}\eta\sigma\rangle$ in Ref. 30, we can estimate s-f integrals as follows:

$$\langle \boldsymbol{i}s|H_{\rm hyb}|\boldsymbol{j}xyz\rangle = \sqrt{15} lmn (sf\sigma), \tag{5}$$

$$\langle \boldsymbol{i}s|H_{\rm hyb}|\boldsymbol{j}x(5x^2 - 3r^2)\rangle = \tfrac{1}{2} l(5l^2 - 3)(sf\sigma), \tag{6}$$

$$\langle \boldsymbol{i}s|H_{\rm hyb}|\boldsymbol{j}x(y^2 - z^2)\rangle = \tfrac{1}{2}\sqrt{15} l(m^2 - n^2)(sf\sigma), \tag{7}$$

where l,m,n are the direction cosine of the vector $\boldsymbol{i}$-$\boldsymbol{j}$. The factor of $\langle \boldsymbol{j}\eta\sigma|\boldsymbol{j}m\sigma\rangle$ corresponds to the weight of spherical harmonics in cubic harmonics. $\langle \boldsymbol{j}m\sigma|\boldsymbol{j}\, j = \frac{5}{2}\mu\rangle$ is merely the Clebsch-Gordan coefficient. The last factor of $\langle \boldsymbol{j}\, j = \frac{5}{2}\mu|\boldsymbol{j}\gamma\tau\rangle$ of Eq. (4) is the weight of $|j = 5/2\mu\rangle$ in $|\gamma\tau\rangle$. Using the bases in the cubic crystalline electric field for $|\gamma\tau\rangle$, we obtain the table of $\langle \eta\sigma|\gamma\tau\rangle$ in Table I.

Next, we specify the hybridization process as the orbital of the conduction electron is situated at the same position as the case of 6s-electron states of rare-earth ions, thus there is no local hybridization between s and f electrons. Therefore, the main hybridization process results from the nearest-neighbor

TABLE I. $\langle \eta\sigma|\gamma\tau\rangle$. η describes a cubic harmonic oscillator. The wave function of $|\gamma\tau\rangle$ is chosen by those of $j = 5/2$ in the cubic crystal structure.

$\eta\sigma \setminus \gamma\tau$	Γ_7+	Γ_7-	$\Gamma_{8(1)}+$	$\Gamma_{8(1)}-$	$\Gamma_{8(2)}+$	$\Gamma_{8(2)}-$
$A_{2u}\uparrow$	$\sqrt{\frac{3}{7}}\mathrm{i}$	0	0	0	0	0
$T_{1u}\alpha\uparrow$	0	0	0	$-\frac{3}{2\sqrt{7}}$	0	$\frac{\sqrt{3}}{2\sqrt{7}}$
$T_{1u}\beta\uparrow$	0	0	0	$\frac{3}{2\sqrt{7}}\mathrm{i}$	0	$\frac{\sqrt{3}}{2\sqrt{7}}\mathrm{i}$
$T_{1u}\gamma\uparrow$	0	0	0	0	$-\sqrt{\frac{3}{7}}$	0
$T_{2u}\xi\uparrow$	0	$\frac{2}{\sqrt{21}}$	0	$\frac{\sqrt{5}}{2\sqrt{21}}$	0	$\frac{\sqrt{5}}{2\sqrt{7}}$
$T_{2u}\eta\uparrow$	0	$\frac{2}{\sqrt{21}}\mathrm{i}$	0	$\frac{\sqrt{5}}{2\sqrt{21}}\mathrm{i}$	0	$-\frac{\sqrt{5}}{2\sqrt{7}}\mathrm{i}$
$T_{2u}\zeta\uparrow$	$\frac{2}{\sqrt{21}}$	0	$-\frac{\sqrt{5}}{\sqrt{21}}$	0	0	0
$A_{2u}\downarrow$	0	$\sqrt{\frac{3}{7}}\mathrm{i}$	0	0	0	0
$T_{1u}\alpha\downarrow$	0	0	$-\frac{3}{2\sqrt{7}}$	0	$\frac{\sqrt{3}}{2\sqrt{7}}$	0
$T_{1u}\beta\downarrow$	0	0	$-\frac{3}{2\sqrt{7}}\mathrm{i}$	0	$-\frac{\sqrt{3}}{2\sqrt{7}}\mathrm{i}$	0
$T_{1u}\gamma\downarrow$	0	0	0	0	0	$\sqrt{\frac{3}{7}}$
$T_{2u}\xi\downarrow$	$\frac{2}{\sqrt{21}}$	0	$\frac{\sqrt{5}}{2\sqrt{21}}$	0	$\frac{\sqrt{5}}{2\sqrt{7}}$	0
$T_{2u}\eta\downarrow$	$-\frac{2}{\sqrt{21}}\mathrm{i}$	0	$-\frac{\sqrt{5}}{2\sqrt{21}}\mathrm{i}$	0	$\frac{\sqrt{5}}{2\sqrt{7}}\mathrm{i}$	0
$T_{2u}\zeta\uparrow$	0	$-\frac{2}{\sqrt{21}}$	0	$\frac{\sqrt{5}}{\sqrt{21}}$	0	0

hopping from the f-electron state at a site $\boldsymbol{i}$ to the s-electron state at a neighboring site $\boldsymbol{i}+e$, where e is a vector connecting with a neighboring unit cell.

Using the hybridization matrix discussed above, we obtain the matrix element for the hopping to the (100) direction,

$$\begin{aligned}\langle \boldsymbol{i}+xs\uparrow|H_{\mathrm{hyb}}|\boldsymbol{i}\Gamma_{8(1)}-\rangle &= \langle \boldsymbol{i}+xs\downarrow|H_{\mathrm{hyb}}|\boldsymbol{i}\Gamma_{8(1)}+\rangle \\ &= -\frac{3}{2\sqrt{7}}(sf\sigma), \end{aligned} \tag{8}$$

$$\begin{aligned}\langle \boldsymbol{i}+xs\uparrow|H_{\mathrm{hyb}}|\boldsymbol{i}\Gamma_{8(2)}-\rangle &= \langle \boldsymbol{i}+xs\downarrow|H_{\mathrm{hyb}}|\boldsymbol{i}\Gamma_{8(2)}+\rangle \\ &= \frac{\sqrt{3}}{2\sqrt{7}}(sf\sigma); \end{aligned} \tag{9}$$

for the hopping to the (010) direction,

$$\begin{aligned}\langle \boldsymbol{i}+ys\uparrow|H_{\mathrm{hyb}}|\boldsymbol{i}\Gamma_{8(1)}-\rangle &= -\langle \boldsymbol{i}+ys\downarrow|H_{\mathrm{hyb}}|\boldsymbol{i}\Gamma_{8(1)}+\rangle \\ &= \frac{3}{2\sqrt{7}}\mathrm{i}(sf\sigma), \end{aligned} \tag{10}$$

$$\begin{aligned}\langle \boldsymbol{i}+ys\uparrow|H_{\mathrm{hyb}}|\boldsymbol{i}\Gamma_{8(2)}-\rangle &= -\langle \boldsymbol{i}+ys\downarrow|H_{\mathrm{hyb}}|\boldsymbol{i}\Gamma_{8(2)}+\rangle \\ &= \frac{\sqrt{3}}{2\sqrt{7}}\mathrm{i}(sf\sigma); \end{aligned} \tag{11}$$

and for the hopping to the (001) direction,

$$\begin{aligned}\langle \boldsymbol{i}+zs\uparrow|H_{\mathrm{hyb}}|\boldsymbol{i}\Gamma_{8(2)}+\rangle &= -\langle \boldsymbol{i}+zs\downarrow|H_{\mathrm{hyb}}|\boldsymbol{i}\Gamma_{8(2)}-\rangle \\ &= -\sqrt{\frac{3}{7}}(sf\sigma), \end{aligned} \tag{12}$$

respectively.

Introducing $V_{sf} = \frac{\sqrt{3}}{2\sqrt{7}}(sf\sigma)$ for simplicity, we obtain the hybridization Hamiltonian to the (100) direction as

$$\begin{aligned}H_{\mathrm{hyb}}^{(100)} = V_{sf}\sum_{\boldsymbol{k}}\Bigg(&[c_{\boldsymbol{k}\uparrow}^\dagger \quad c_{\boldsymbol{k}\downarrow}^\dagger]\begin{bmatrix}0 & 2\sqrt{3}\mathrm{i}\sin k_x\\ 2\sqrt{3}\mathrm{i}\sin k_x & 0\end{bmatrix}\begin{bmatrix}f_{\boldsymbol{k}\Gamma_{8(1)}+}\\ f_{\boldsymbol{k}\Gamma_{8(1)}-}\end{bmatrix}\\ &+[c_{\boldsymbol{k}\uparrow}^\dagger \quad c_{\boldsymbol{k}\downarrow}^\dagger]\begin{bmatrix}0 & -2\mathrm{i}\sin k_x\\ -2\mathrm{i}\sin k_x & 0\end{bmatrix}\begin{bmatrix}f_{\boldsymbol{k}\Gamma_{8(2)}+}\\ f_{\boldsymbol{k}\Gamma_{8(2)}-}\end{bmatrix}\Bigg) + \mathrm{H.c.}; \end{aligned} \tag{13}$$

for the (010) direction as

$$\begin{aligned}H_{\mathrm{hyb}}^{(010)} = V_{sf}\sum_{\boldsymbol{k}}\Bigg(&[c_{\boldsymbol{k}\uparrow}^\dagger \quad c_{\boldsymbol{k}\downarrow}^\dagger]\begin{bmatrix}0 & 2\sqrt{3}\sin k_y\\ -2\sqrt{3}\sin k_y & 0\end{bmatrix}\begin{bmatrix}f_{\boldsymbol{k}\Gamma_{8(1)}+}\\ f_{\boldsymbol{k}\Gamma_{8(1)}-}\end{bmatrix}\\ &+[c_{\boldsymbol{k}\uparrow}^\dagger \quad c_{\boldsymbol{k}\downarrow}^\dagger]\begin{bmatrix}0 & 2\sin k_y\\ -2\sin k_y & 0\end{bmatrix}\begin{bmatrix}f_{\boldsymbol{k}\Gamma_{8(2)}+}\\ f_{\boldsymbol{k}\Gamma_{8(2)}-}\end{bmatrix}\Bigg) + \mathrm{H.c.}; \end{aligned} \tag{14}$$

and for the (001) direction as

$$H_{\mathrm{hyb}}^{(001)} = V_{sf}\sum_{\boldsymbol{k}}[c_{\boldsymbol{k}\uparrow}^\dagger \quad c_{\boldsymbol{k}\downarrow}^\dagger]\begin{bmatrix}4\mathrm{i}\sin k_z & 0\\ 0 & -4\mathrm{i}\sin k_z\end{bmatrix}\begin{bmatrix}f_{\boldsymbol{k}\Gamma_{8(2)}+}\\ f_{\boldsymbol{k}\Gamma_{8(2)}-}\end{bmatrix} + \mathrm{H.c.} \tag{15}$$

Gathering all these terms, the resulting hybridization Hamiltonian is given by

$$H_{\mathrm{hyb}} = V_{sf}\sum_{\boldsymbol{k}}[c_{\boldsymbol{k}\uparrow}^\dagger \quad c_{\boldsymbol{k}\downarrow}^\dagger]\left(\hat{V}_{\Gamma_{8(1)}}(\boldsymbol{k})\begin{bmatrix}f_{\boldsymbol{k}\Gamma_{8(1)}+}\\ f_{\boldsymbol{k}\Gamma_{8(1)}-}\end{bmatrix} + \hat{V}_{\Gamma_{8(2)}}(\boldsymbol{k})\begin{bmatrix}f_{\boldsymbol{k}\Gamma_{8(2)}+}\\ f_{\boldsymbol{k}\Gamma_{8(2)}-}\end{bmatrix}\right) + \mathrm{H.c.}, \tag{16}$$

where the hybridization matrix

$$\hat{V}_\Gamma(\boldsymbol{k}) = \boldsymbol{d}_\Gamma(\boldsymbol{k}) \cdot \hat{\boldsymbol{\sigma}} \tag{17}$$

is

$$\boldsymbol{d}_{\Gamma_{8(1)}}(\boldsymbol{k}) = (2\sqrt{3}\mathrm{i}\sin k_x, 2\sqrt{3}\mathrm{i}\sin k_y, 0), \tag{18}$$

$$\boldsymbol{d}_{\Gamma_{8(2)}}(\boldsymbol{k}) = (-2\mathrm{i}\sin k_x, 2\mathrm{i}\sin k_y, 4\mathrm{i}\sin k_z). \tag{19}$$

We note that this model Hamiltonian describes the nearest-neighbor hybridization process between s and f electrons of rare-earth ions in the simple-cubic lattice. In Appendix A, we discuss how the hybridization Hamiltonian is modified when the lattice symmetry is lowered from the simple cubic to the tetragonal.

B. U(1) slave-boson mean-field analysis

We start from an effective Anderson lattice model,

$$\begin{aligned} H = &\sum_{\boldsymbol{k}}\sum_{\sigma}\left(\varepsilon^c_{\boldsymbol{k}} - \mu_c\right)c^\dagger_{\boldsymbol{k}\sigma}c_{\boldsymbol{k}\sigma} + \sum_{i}\sum_{\alpha}(\epsilon_f - \mu_c)f^\dagger_{i\alpha}f_{i\alpha} \\ &- \epsilon\sum_{ij}\sum_{\alpha\alpha'}t_{ij\alpha\alpha'}f^\dagger_{i\alpha}f_{j\alpha'} + \frac{U}{2}\sum_{i}\sum_{\alpha}f^\dagger_{i\alpha}f_{i\alpha}f^\dagger_{i-\alpha}f_{i-\alpha} \\ &+ V\sum_{\boldsymbol{k}}\sum_{i}\sum_{\alpha\sigma}[\boldsymbol{d}_\Gamma(\boldsymbol{k})\cdot\hat{\boldsymbol{\sigma}}_{\sigma\alpha}c^\dagger_{\boldsymbol{k}\sigma}f_{i\alpha}e^{-i\boldsymbol{k}\cdot\boldsymbol{r}_i} + \mathrm{H.c.}], \end{aligned} \tag{20}$$

where $t_{ij\alpha\alpha'}$ is the hopping integral of f electrons with a parameter $\epsilon \ll 1$ and the subscript sf in V_{sf} is omitted for simplicity. This effective hopping for localized fermions is introduced phenomenologically to describe possible phase transitions from the "fractionalized' Fermi-liquid state[31] to the Kondo insulating phase at zero temperature, which can be regarded as resulting from Ruderman-Kittel-Kasuya-Yoshida (RKKY) spin correlations effectively in an intermediate energy scale.[32] The hybridization coupling term is given by Eqs. (18) and (19) for the simple-cubic case.[33]

We take the U(1) slave-boson representation for the Kondo effect in the strong-coupling limit, where the localized fermion is expressed as $f_{i\alpha} \to b^\dagger_i f_{i\alpha}$ with the single occupancy constraint $b^\dagger_i b_i + \sum_{\alpha=\pm} f^\dagger_{i\alpha}f_{i\alpha} = 1$. Then, the effective Lagrangian is given by

$$\begin{aligned} L = &\sum_{\boldsymbol{k}}\sum_{\sigma}c^\dagger_{\boldsymbol{k}\sigma}\left(\partial_\tau - \mu_c + \varepsilon^c_{\boldsymbol{k}}\right)c_{\boldsymbol{k}\sigma} + V\sum_{\boldsymbol{k}}\sum_{i}\sum_{\alpha\sigma} \\ &\times[\boldsymbol{\Phi}_{\alpha\sigma}(\boldsymbol{k})c^\dagger_{\boldsymbol{k}\sigma}b^\dagger_i f_{i\alpha}e^{-i\boldsymbol{k}\cdot\boldsymbol{r}_i} + \mathrm{H.c.}] \\ &+ \sum_{i}\sum_{\alpha}f^\dagger_{i\alpha}(\partial_\tau + \epsilon_f - \mu_c + i\lambda_i)f_{i\alpha} \\ &- \epsilon\sum_{ij}\sum_{\alpha\alpha'}t_{ij\alpha\alpha'}f^\dagger_{i\alpha}b^\dagger_i b_j f_{j\alpha'} + i\sum_i\lambda_i(b^\dagger_i b_i - 1), \end{aligned} \tag{21}$$

where λ_i is the Lagrange multiplier field for the constraint and $\boldsymbol{\Phi}_{\alpha\sigma}(\boldsymbol{k}) \equiv \boldsymbol{d}_\Gamma(\boldsymbol{k})\cdot\hat{\boldsymbol{\sigma}}_{\sigma\alpha}$.

Taking $b_i \to b \equiv \langle b_i\rangle$ with $i\lambda_i \to \lambda$ in the saddle-point approximation, we obtain two self-consistent equations for b and λ, given by

$$\begin{aligned} \lambda = V^2\sum_{\boldsymbol{k}}\sum_{\alpha\alpha'\sigma}\boldsymbol{\Phi}_{\alpha\sigma}(\boldsymbol{k})\boldsymbol{\Phi}^*_{\alpha'\sigma}(\boldsymbol{k})\frac{1}{\pi}\int_{-\infty}^{\infty}d\omega n_F(\omega)\mathrm{Im} \\ \times\frac{G^f_{\alpha\alpha'}(\omega + i0^+, \boldsymbol{k})}{\omega - \varepsilon^c_{\boldsymbol{k}} + \mu_c + i0^+}, \end{aligned} \tag{22}$$

$$b^2 - \frac{1}{\pi}\sum_{\boldsymbol{k}}\sum_{\alpha}\int_{-\infty}^{\infty}d\omega n_F(\omega)\mathrm{Im}G^f_{\alpha\alpha}(\omega + i0^+, \boldsymbol{k}) = 1, \tag{23}$$

respectively. $\boldsymbol{G}^f(\omega, \boldsymbol{k})$ is the spinon Green's function, given by

$$\begin{aligned} \boldsymbol{G}^f(\omega, \boldsymbol{k}) = \Big[&(\omega - \epsilon_f + \mu_c - \lambda)\mathbf{1} + \epsilon\boldsymbol{t}(\boldsymbol{k}) \\ &- V^2b^2\frac{\boldsymbol{\Phi}(\boldsymbol{k})\cdot\boldsymbol{\Phi}^*(\boldsymbol{k})}{\omega - \varepsilon^c_{\boldsymbol{k}} + \mu_c}\Big]^{-1}, \end{aligned} \tag{24}$$

where $[\boldsymbol{t}(\boldsymbol{k})]_{\alpha\alpha'} \equiv \sum_{ij}[\boldsymbol{t}_{ij}]_{\alpha\alpha'}\exp[i\boldsymbol{k}\cdot(\boldsymbol{r}_i - \boldsymbol{r}_j)]$. $n_F(\omega) = 1/[\exp(\omega/T) + 1]$ is the Fermi-Dirac distribution function.

C. Phase diagram

It is natural to expect a phase transition from the fractionalized Fermi liquid to the Kondo insulating state, described by the emergence of the Kondo effect ($b \neq 0$) above a critical strength of hybridization. An interesting aspect of this effective lattice model is that there can exist additional phase transitions inside the Kondo-insulating phase, not described by the holon condensation but characterized by the change of the Z_2 topological index.

For simplicity, we take $\boldsymbol{t}_{\alpha\alpha'}(\boldsymbol{k}) = \delta_{\alpha\alpha'}t(\boldsymbol{k})$ with $t(\boldsymbol{k}) = \varepsilon^c_{\boldsymbol{k}}$. Introduction of the spin dependence will not change possible phases but will modify critical values of V associated with their phase transitions. The dispersion relations for the heavy-fermion bands are given by

$$\begin{aligned} E_\pm(\boldsymbol{k}) = &\tfrac{1}{2}\left[\varepsilon^c_{\boldsymbol{k}} - \epsilon t(\boldsymbol{k}) + \epsilon_f + \lambda\right] - \mu_c \\ &\pm\tfrac{1}{2}\sqrt{\left[\varepsilon^c_{\boldsymbol{k}} + \epsilon t(\boldsymbol{k}) - \epsilon_f - \lambda\right]^2 + 4V^2b^2\Delta^2(\boldsymbol{k})}, \end{aligned} \tag{25}$$

respectively, where $\Delta^2(\boldsymbol{k}) = \frac{1}{2}\mathrm{Tr}[\boldsymbol{\Phi}(\boldsymbol{k})\cdot\boldsymbol{\Phi}^\dagger(\boldsymbol{k})]$.

In order to see how the band inversion occurs from this dispersion relation, we consider time-reversal-invariant momenta that satisfy $\boldsymbol{k}^*_m = -\boldsymbol{k}^*_m + \boldsymbol{G}$, where $\boldsymbol{G}$ is a reciprocal-lattice vector. It is straightforward to check that there are eight time-reversal-invariant momentum points in three dimensions while there are four in two dimensions. The Z_2 topological index, which measures how many times bands are twisted with modular 2, has been reformulated for such time-reversal-invariant momenta in the case in which the system preserves the inversion symmetry.[9–11] First, we observe that the band gap in the Kondo insulating phase closes linearly at some of the time-reversal symmetry points which satisfy $\epsilon_f + \lambda = \varepsilon^c_{\boldsymbol{k}^*_m} + \epsilon t(\boldsymbol{k}^*_m)$, where $\Delta(\boldsymbol{k}) \sim |\boldsymbol{k}|$ appears near $\boldsymbol{k}^*_m$. This identification leads us to define the parity $\delta_m = \mathrm{sgn}[\varepsilon^c_{\boldsymbol{k}^*_m} + \epsilon t(\boldsymbol{k}^*_m) - \epsilon_f - \lambda]$. See Appendix B. Following Dzero *et al.*,[28] we can evaluate the Z_2 topological indices given by

$$I_{\mathrm{STI}} = \prod_m \delta_m, \tag{26}$$

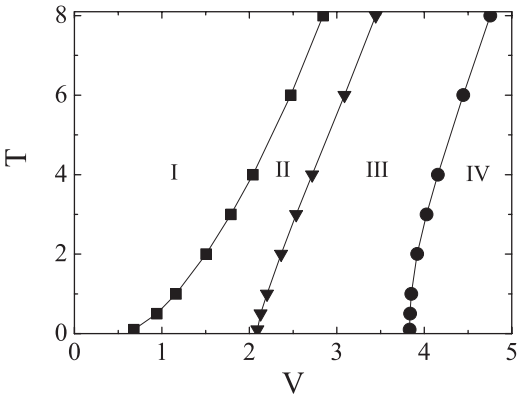

FIG. 1. U(1) slave-boson mean-field phase diagram for an effective Anderson lattice model with the $\Gamma_{8(2)}$ hybridization on the simple-cubic lattice. Phase I is the fractionalized Fermi-liquid state, where localized spins are decoupled from conduction electrons ($b = 0$) forming a spinon "Fermi'-liquid state (spin liquid). The Kondo insulating phase ($b \neq 0$) is separated into phase II, phase III, and phase IV, classified by the topological Z_2 indices. Phase II is the weak topological Kondo insulator and phase III is the strong topological Kondo insulator. Phase IV is the normal Kondo insulator. The first transition belongs to the second order in the saddle-point approximation, but fluctuation corrections might change the nature of the continuous transition to first order. On the other hand, phase transitions inside the Kondo insulator are also continuous, but are regarded as robust against quantum corrections, where both hybridization and gauge fluctuations are irrelevant. The topological aspect of the band structure is changed by the gap closing transition. Model parameters of $t = 1$, $\epsilon = 0.005$, $\epsilon_f = -6$, and $\mu_c = 0$ are used.

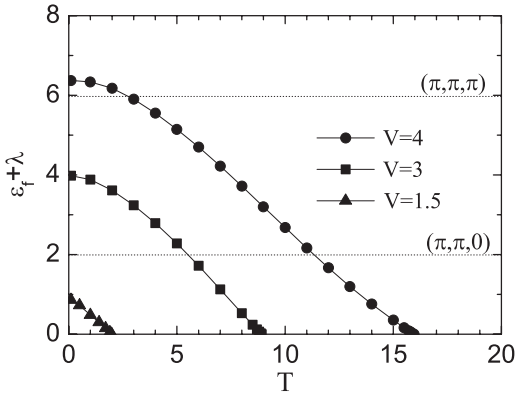

FIG. 2. Temperature dependence of the renormalized orbital energy $\epsilon_f + \lambda$ for various values of V. Dotted lines indicate the value of $\varepsilon^c_{k^*_m} + \epsilon t(k^*_m)$ at time-reversal-invariant points. In this figure, it is straightforward to see changes of Z_2 topological indices, where the Chern parity can be evaluated automatically. Model parameters of $t = 1$, $\epsilon = 0.005$, $\epsilon_f = -6$, and $\mu_c = 0$ are used.

$$I^{\alpha}_{\mathrm{WTI}} = \prod_m \delta_m \Big|_{(\boldsymbol{k}^*_m)_\alpha = 0}, \tag{27}$$

where I_{STI} is an index for a strong topological insulator while $I^{\alpha}_{\mathrm{WTI}}$ are indices for a weak topological insulator. We will see these indices changed, showing additional phase transitions inside the Kondo insulator.

We solve the mean-field equations (22) and (23) with (24) for the simple-cubic lattice with

$$\varepsilon^c_{\boldsymbol{k}} = -t(\boldsymbol{k}) = -2t(\cos k_x + \cos k_y + \cos k_z) \tag{28}$$

numerically, and we take the hybridization term of the $\Gamma_{8(2)}$ symmetry. Our slave-boson analysis uncovers four different phases in three dimensions, shown in Fig. 1. When the hybridization coupling is smaller than a critical value V_c, the Kondo effect does not exist, i.e., $b = 0$ (phase I), giving rise to local magnetic moments decoupled from conduction electrons, where such localized spins form a spinon "Fermi'-liquid state (spin liquid) due to their dispersions originating from the RKKY interaction.[31] Such an exotic liquid state may be realized in geometrically frustrated lattices or at finite temperatures.[34] Increasing the hybridization coupling above V_c, the Kondo effect results in the formation of the heavy-fermion band ($b \neq 0$), but the condition of half-filling for conduction electrons leads to an insulating state instead of the heavy-fermion metal. An interesting point is that the Kondo insulating state can be separated into three insulating phases, classified by the Z_2 topological indices. Phase II is characterized by the trivial strong topological-insulator index of $I_{\mathrm{STI}} = 1$, but nontrivial weak topological-insulator indices of $I^x_{\mathrm{WTI}} = I^y_{\mathrm{WTI}} = I^z_{\mathrm{WTI}} = -1$. Thus, phase II is identified by the weak topological Kondo insulator. Phase III is characterized by $I_{\mathrm{STI}} = -1$ and $I^x_{\mathrm{WTI}} = I^y_{\mathrm{WTI}} = I^z_{\mathrm{WTI}} = 1$. As a result, it is the strong topological Kondo insulator. The last Kondo insulating phase, phase IV, is the conventional Kondo insulator with trivial Z_2 indices of $I_{\mathrm{STI}} = 1$ and $I^x_{\mathrm{WTI}} = I^y_{\mathrm{WTI}} = I^z_{\mathrm{WTI}} = 1$.

It is straightforward to see changes of Z_2 topological indices in Fig. 2, where the Chern parity can be evaluated automatically. For example, if one fixes $V = 3t$ and lowers temperature, he can find a continuous phase transition from the weak topological Kondo insulating state (phase II) to the strong topological Kondo insulating phase (phase III) around $T \approx 5t$. If one considers $V = 4t$, he can observe two continuous phase transitions (i) from the weak topological Kondo insulating state (phase II) to the strong topological Kondo insulating phase (phase III) around $T \approx 11t$ and (ii) from the strong topological Kondo insulating state (phase III) to the nontopological Kondo insulating phase (phase IV) around $T \approx 3t$. Figure 3 shows the phase transition from the fractionalized Fermi liquid state (phase I) to the weak topological Kondo insulating phase (phase II) at each temperature, depending on the value of the hybridization coupling constant. Figures 2 and 3 show how we obtain the phase diagram, Fig. 1.

Since the first phase transition from the fractionalized Fermi liquid to the weak topological Kondo insulator is given by the holon condensation, i.e., the formation of the Kondo effect, it belongs to the second-order transition in the saddle-point approximation. Two more phase transitions inside the Kondo insulator are described by gap closing, thus they also belong to the continuous transition. An important point is that such second-order transitions inside the Kondo insulating phase are expected to be robust because singular corrections from fluctuations will not exist inside the Kondo insulator. In particular, both hybridization and gauge fluctuations will not play an important role in these phase transitions. On the other hand, such quantum corrections may be important for the

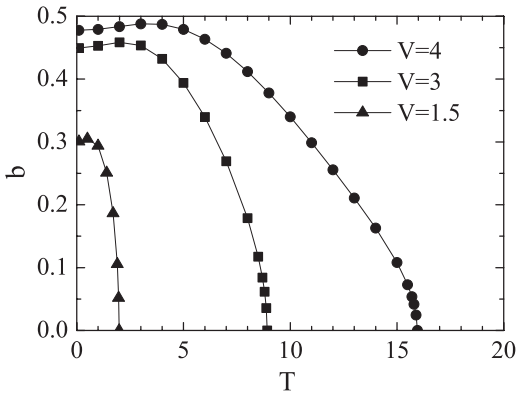

FIG. 3. Temperature dependence of the boson-condensation amplitude for various values of V. This figure determines the phase transition from the fractionalized Fermi liquid state (phase I) to the weak topological Kondo insulating phase (phase II) at each temperature, depending on the value of the hybridization coupling constant. Model parameters of $t = 1$, $\epsilon = 0.005$, $\epsilon_f = -6$, and $\mu_c = 0$ are used.

nature of the first phase transition from the fractionalized Fermi liquid to the weak topological Kondo insulator, which will be discussed in the final section.

It is straightforward to check the two-dimensional case, i.e., the effective Anderson lattice model on the square lattice. Indeed, we performed the same slave-boson mean-field analysis in two dimensions and found the corresponding phase diagram of Fig. 4. The main difference from the three-dimensional case is the absence of the strong topological Kondo insulating phase, where the quantum "spin' Hall Kondo-insulating phase exists between the fractionalized Fermi liquid and the normal Kondo insulator. Figure 5 displays the band structures of both the topological (normal) Kondo insulating phase and the critical point, where the gap closing occurs at $\boldsymbol{k}^*_{\pi\pi} = (\pi,\pi)$.

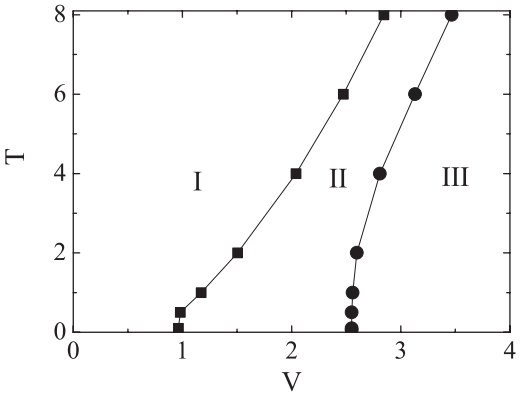

FIG. 4. U(1) slave-boson mean-field phase diagram for an effective Anderson lattice model with the $\Gamma_{8(1)}$ hybridization and $\boldsymbol{k}_z = 0$, i.e., on the square lattice. Phase I is the fractionalized Fermi-liquid state ($b = 0$), phase II is the topological Kondo insulator ($b \neq 0$ and $I^z_{\rm WTI} = -1$), and phase III is the normal Kondo insulator ($b \neq 0$ and $I^z_{\rm WTI} = 1$). Model parameters of $t = 1, \epsilon = 0.005, \epsilon_f = -6$, and $\mu_c = 0$ are used.

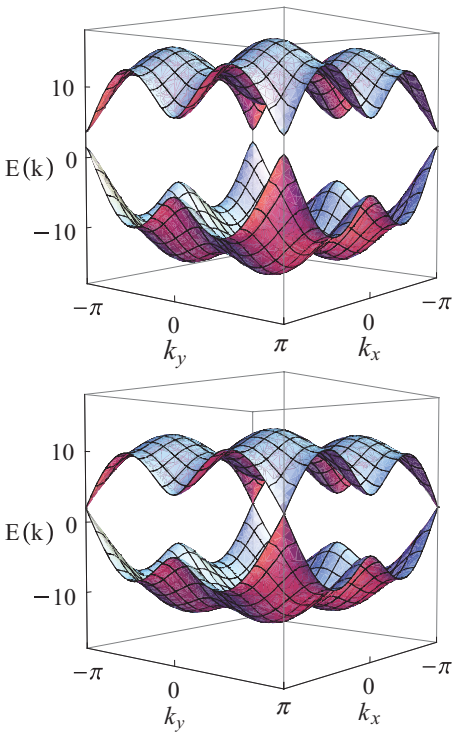

FIG. 5. (Color online) Top: The band structure in the Kondo insulating state (phase III). It is almost identical to that in the topological Kondo insulating phase (phase II). The electron chemical potential lies between the band gap. Bottom: The band structure at the critical point inside the Kondo insulator. Gap closing appears at $\boldsymbol{k}^*_{\pi\pi} = (\pi,\pi)$, described by the Dirac theory from Eq. (31) to Eq. (39) with $\boldsymbol{k}_z = 0$. Model parameters of $t = 1, \epsilon = 0.005$, and $\epsilon_f = -6$ are used.

D. Comparison with the previous study

One may wonder what the differences are between the present study and the previous seminal work.[28] The mechanism itself for the emergence of the topological Kondo insulator is essentially the same. However, we emphasize that our phase diagram differs from the previous one in that Fig. 1 is shown in the plane of (V,T) while the previous study displays its phase diagram as a function of the renormalized orbital energy $\epsilon_f + \lambda$ at $T = 0$. In particular, Fig. 1 with Fig. 2 shows us a general feature for the emergence of the topological Kondo insulating phase, at least where it should occur just before the normal Kondo insulating phase. Figure 2 displays the change of the parity δ_m as temperature decreases with various values of V. Considering how the $\epsilon_f + \lambda(V,T)$ curve cuts $\varepsilon^c_{k^*_m} + \epsilon t(k^*_m)$ at various time-reversal-invariant momentum points k^*_m in Fig. 2, one can realize that the topological Kondo insulating phase will appear before the normal Kondo insulating phase.

The two studies use different methods to analyze this problem, although this difference does not seem to be crucial. Basically, we need two "order parameters' for the self-consistent mean-field analysis of this problem. In the slave-boson approach, we have the condensation amplitude of the hybridization order parameter b and the effective chemical potential $\epsilon_f + \lambda$ for localized electrons, which correspond to the quasiparticle weight (the wave-function renormalization constant) Z and the renormalized orbital energy in the previous study.[28] Investigating the previous study carefully, we suspect

that the analysis may not be fully self-consistent because the previous study uses the renormalized orbital energy as an external parameter for the phase diagram, while it should be determined self-consistently. Although this can be easily fixed, this is one difference in the analysis. In this respect, we draw a phase diagram, Fig. 6, in the plane of (V,ϵ_f) at low temperature, recovering and extending the phase diagram of Ref. 28.

E. An effective Dirac theory for the hybridization coupling with the symmetry $\Gamma_{8(1)}$

The Dirac theory gives an effective field theory for the phase transition from the strong topological Kondo insulator to the normal Kondo insulator. The effective slave-boson Hamiltonian for the topological Kondo insulator is

$$H = \sum_{\boldsymbol{k}} \Psi_{\boldsymbol{k}}^{\dagger} H(\boldsymbol{k}) \Psi_{\boldsymbol{k}} + \lambda(b^2 - 1), \tag{29}$$

$$H(\boldsymbol{k}) = \begin{pmatrix} \varepsilon_{\boldsymbol{k}}^{c} - \mu_c & Vb\Phi(\boldsymbol{k}) & 0 & 0 \\ Vb\Phi^*(\boldsymbol{k}) & -\epsilon t(\boldsymbol{k}) + \widetilde{\epsilon}_f - \mu_c & 0 & 0 \\ 0 & 0 & \varepsilon_{\boldsymbol{k}}^{c} - \mu_c & -Vb\Phi^*(\boldsymbol{k}) \\ 0 & 0 & -Vb\Phi(\boldsymbol{k}) & -\epsilon t(\boldsymbol{k}) + \widetilde{\epsilon}_f - \mu_c \end{pmatrix}, \tag{30}$$

where $\Psi_{\mathbf{k}}^{\dagger} = (c_{\mathbf{k}\uparrow}^{\dagger}, f_{\mathbf{k}-}^{\dagger}, c_{\mathbf{k}\downarrow}^{\dagger}, f_{\mathbf{k}+}^{\dagger})$ is the four-component Dirac spinor with $\widetilde{\epsilon}_f = \epsilon_f + \lambda$, and $\Phi(\mathbf{k}) = 2\sqrt{3}i \sin k_x + 2\sqrt{3} \sin k_y$ is the form factor of the $\Gamma_{8(1)}$ hybridization.

Expanding $H(\boldsymbol{k})$ around the gap closing point with time-reversal symmetry, $\boldsymbol{k}^*_{\pi\pi\pi} = (\pi,\pi,\pi)$, we obtain an effective Dirac theory

$$H(\boldsymbol{p}) = \begin{pmatrix} h(\boldsymbol{p}) & 0 \\ 0 & h^*(-\boldsymbol{p}) \end{pmatrix}, \tag{31}$$

where $h(\boldsymbol{p}) = \varepsilon(\boldsymbol{p})\sigma_0 + \boldsymbol{d}(\boldsymbol{p}) \cdot \boldsymbol{\sigma}$ is the two-by-two Dirac Hamiltonian with

$$\varepsilon(\boldsymbol{p}) = C - D\left(p_x^2 + p_y^2 + p_z^2\right), \tag{32}$$

$$\boldsymbol{d}(\boldsymbol{p}) = (Ap_y, Ap_x, M(\boldsymbol{p})), \tag{33}$$

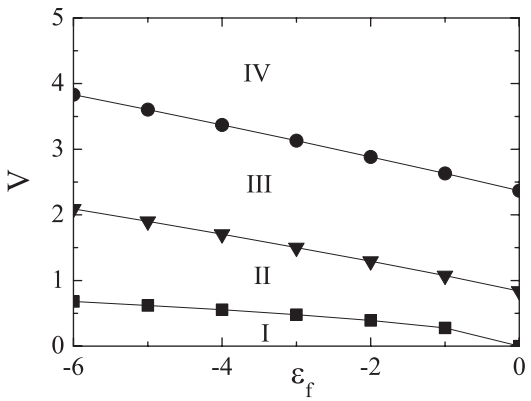

FIG. 6. Phase diagram for the $\Gamma_{8(2)}$ hybridization at temperature $T = 0.1t$. Phase I is the fractionalized Fermi-liquid state, phase II is the weak topological Kondo insulator, phase III is the strong topological Kondo insulator, and phase IV is the normal Kondo insulator. Model parameters of $t = 1$, $\epsilon = 0.005$, and $\mu_c = 0$ are used.

$$M(\boldsymbol{p}) = M - B\left(p_x^2 + p_y^2 + p_z^2\right), \tag{34}$$

$$C = 3t + \frac{3}{2}\epsilon + \frac{1}{2}\widetilde{\epsilon}_f - \mu_c, \tag{35}$$

$$D = \frac{1}{2}\left(t + \frac{\epsilon}{2}\right), \tag{36}$$

$$A = -2\sqrt{3}Vb, \tag{37}$$

$$B = \frac{1}{2}\left(t - \frac{\epsilon}{2}\right), \tag{38}$$

$$M = 3t - \frac{3}{2}\epsilon - \frac{1}{2}\widetilde{\epsilon}_f. \tag{39}$$

This effective Hamiltonian turns out to be identical with that of Ref. 35 when $p_x \to p_y$ and $p_y \to p_x$ are performed with $p_z = 0$. The spectrum is

$$E_{\pm}(\boldsymbol{p}) = \varepsilon(\boldsymbol{p}) \pm \sqrt{A^2\left(p_x^2 + p_y^2\right) + M^2(\boldsymbol{p})}. \tag{40}$$

Note that $\mathrm{sgn}(M) = \delta_{\boldsymbol{k}^*_{\pi\pi\pi}}$ corresponds to the parity at the symmetry point $\boldsymbol{k}^*_{\pi\pi\pi} = (\pi,\pi,\pi)$. Recall that the Chern number is given by $\mathcal{C} = 1$ for $M/B > 0$ and $\mathcal{C} = 0$ for $M/B < 0$ in the two-dimensional case. This means that the parity $\delta_{\boldsymbol{k}^*_{\pi\pi\pi}}$ describes the transition from the topological insulator to the trivial insulator via gap closing.

In Appendix C, we derive an effective Dirac theory for the case of hybridization with $\Gamma_{8(2)}$.

III. SUMMARY AND DISCUSSION

It is essential to construct realistic lattice models when researching novel quantum states of matter. In this study, we construct an effective Anderson lattice model in order to study an interplay between the topological aspect and strong correlation, regarded as two cornerstones for novel quantum states of matter. The topological structure could be introduced in the spin-pseudospin–dependent hybridization

between conduction electrons and localized electrons, which originates from the interplay between the spin-orbit interaction and crystalline electric field for localized f electrons. The spin-pseudospin–dependent Kondo effect plays essentially the same role as the spin-orbit coupling for topological insulators, allowing the topological Kondo insulator inside the Kondo insulating phase. Although its existence was already pointed out in an interesting recent study,[28] our detailed slave-boson analysis has clarified its position in the phase diagram. In addition, we can argue that the existence of the topological Kondo insulating phase is robust against quantum corrections because hybridization fluctuations cannot be strong inside the Kondo insulator, and gauge fluctuations are not either.

Unfortunately, it is difficult to say that such topological states are quite interesting because the appearance of the topological Kondo insulator just comes from the inversion of heavy-fermion bands, basically the same as that in topological insulators of noninteracting electrons. However, we would like to point out that the present effective lattice model has a huge potential for novel quantum states of matter. In particular, we expect interesting spin-ordering structures in the position of the fractionalized Fermi liquid state, which results from the underestimation of spin correlations in the slave-boson approach. In this respect, the saddle-point analysis based on the slave-fermion theory[36] will open the possibility of fruitful spin structures, where exotic ordering of localized spins may appear as a result of the spin-dependent Kondo effect. Recently, the integer quantum Hall effect was proposed in the ferromagnetically Kondo coupled lattice model on geometrically frustrated lattices,[37] where the kinetic-energy cost for conduction electrons becomes reduced due to the emergence of an internal magnetic flux from the formation of the spin chirality order. In addition, it is natural to expect the possibility of novel quantum criticality between the fractionalized Fermi liquid and the topological Kondo insulator because the band inversion occurs with the formation of the heavy-fermion band at the same time, quite uncommon in the Landau-Ginzburg-Wilson description for phase transitions. Of course, anomalous scaling near this quantum criticality is expected to be beyond the scope of the present mean-field analysis. Recently, two of us constructed an Eliashberg theory for the spin-density-wave transition in the surface state of the three-dimensional topological insulator,[38] where the band reconstruction is not introduced but fluctuation corrections are incorporated. In this study, we uncovered that the anomalous self-energy correction (the of-diagonal self-energy in the spin or pseudospin space) is essential for self-consistency. We speculate that mathematically the same self-energy correction via hybridization fluctuations will play an important role for this nontrivial quantum criticality. In particular, we expect that the characteristic feature for this quantum critical point may be introduced in scaling of the anomalous Hall conductivity. Numerical simulations for this model seem to be invaluable.

One may wonder what the role is of finite U in the Anderson lattice model instead of the $U \to \infty$ limit, where double occupancy is allowed to cause additional charge fluctuations, which differ from those due to hybridization with conduction electrons. The slave-rotor representation has been developed to describe the Mott transition from a spin liquid to a Fermi liquid,[39–41] where charge fluctuations from double occupancy are taken into account. If we try to apply this methodology to the Anderson lattice model, we face the difficulty of having to deal with the hybridization coupling term. When we treat such a term introducing condensation of the rotor field, the result will be basically the same as the slave-boson approach of the present model. On the other hand, if we introduce the Kondo effect from an uncondensed phase as the "conventional' slave-rotor approach,[39,41] we need to take quantum corrections from the hybridization term fully self-consistently at least in the one-loop level. Then, we can perform the standard "mean-field' analysis with such a *modified* slave-rotor theory. However, this procedure contains additional self-consistent equations for self-energy corrections beyond the standard slave-rotor analysis that are more complicated and beyond the scope of the present issue, i.e., the phase structure of the topological Kondo insulating system. However, this is an important and fundamental problem in that the nature of an orbital-selective Mott transition in the Anderson lattice model[32] may differ from the Mott transition of the Hubbard model. This deserves to be studied more carefully in the near future.

Recently, SmB_6 has been suggested to belong to a class of topological Kondo insulators.[42] However, it has not been completely confirmed yet whether this Kondo semiconductor is or can become a topological insulator. The existence of the so-called "in-gap' states makes the problem difficult. Actually, the origin of in-gap states is still controversial,[43] although the in-gap states have been observed by various experimental measurements such as resistivity, optical conductivity, neutron scattering, specific heat, and NMR relaxation rate. Other than these experimental measurements, more elaborate observations for fingerprints, intrinsic in topological insulators only, should be made to distinguish the topological aspect of systems.

ACKNOWLEDGMENTS

This work was supported by a National Research Foundation of Korea (NRF) grant funded by the Korea government (MEST) (No. 2011-0074542). M.-T. was also supported by the National Foundation for Science and Technology Development (NAFOSTED) of Vietnam.

APPENDIX A: MODEL HAMILTONIAN IN TETRAGONAL SURROUNDINGS

We consider the effect of symmetry lowering from cubic to tetragonal. In the cubic crystal structure, the level scheme of the f electron for the $j = 5/2$ multiplet is given by

$$D^{5/2}\downarrow O_h = \Gamma_7 \oplus \Gamma_8,$$

which serves as a basis for the extraction of the hybridization Hamiltonian. In the tetragonal surroundings, the $\Gamma_7(O_h)$ and $\Gamma_8(O_h)$ bases are reduced,

$$\begin{aligned}\Gamma_7(O_h)\downarrow D_{4h} &= \Gamma_7,\\ \Gamma_{8(1)}(O_h)\downarrow D_{4h} &= \Gamma_7,\\ \Gamma_{8(2)}(O_h)\downarrow D_{4h} &= \Gamma_6,\end{aligned}$$

respectively. Therefore, $\Gamma_7(O_h)$ and $\Gamma_{8(1)}(O_h)$ states can mix in the tetragonal surroundings, while the $\Gamma_{8(2)}(O_h)$ doublet splits from the $\Gamma_8(O_h)$ quartet by the tetragonal crystalline electric field.

Referring to the above discussion, we can imagine a special case in which only one f-electron doublet is relevant to describe the low-energy physics in the tetragonal system. If the relevant doublet belongs to Γ_7 in the tetragonal system, the effective Hamiltonian will be

$$
\begin{aligned}
&H^{\Gamma_7} = H_c + H_f + H^{\Gamma_7}_{\rm hyb},\\
&H_c = \sum_{\boldsymbol{k}}\sum_{\sigma}\left(\varepsilon^c_{\boldsymbol{k}} - \mu_c\right)c^\dagger_{\boldsymbol{k}\sigma}c_{\boldsymbol{k}\sigma},\\
&H_f = \sum_{i}\sum_{\tau}(\epsilon_f - \mu_c)f^\dagger_{i\tau}f_{i\tau} + U\sum_i n_{fi\tau}n_{fi-\tau},\\
&H^{\Gamma_7}_{\rm hyb} = \sum_{\boldsymbol{k}}[c^\dagger_{\boldsymbol{k}\uparrow}\quad c^\dagger_{\boldsymbol{k}\downarrow}]\boldsymbol{d}_{\Gamma_7}(\boldsymbol{k})\cdot\hat{\boldsymbol{\sigma}}\begin{bmatrix}f_{\boldsymbol{k}+}\\ f_{\boldsymbol{k}-}\end{bmatrix} + \text{H.c.},
\end{aligned}
$$

with

$$
\begin{aligned}
&\varepsilon_f = \varepsilon_{f\Gamma_7},\\
&\boldsymbol{d}_{\Gamma_7}(\boldsymbol{k}) = (2\sqrt{3}\mathrm{i}\tilde{V}_{sf}\sin k_x, 2\sqrt{3}\mathrm{i}\tilde{V}_{sf}\sin k_y, 0),\\
&f_{\boldsymbol{k}\tau} = f_{\boldsymbol{k}\Gamma_7\tau},
\end{aligned}
$$

where $\epsilon_{f\Gamma_7}$ is the relevant Γ_7 doublet corresponding to $f_{\boldsymbol{k}\Gamma_7\tau}$, and $\tilde{V}_{sf}$ is affected from the original V_{sf} by the diagonalization in the tetragonal surroundings.

When the relevant doublet is Γ_6, the effective Hamiltonian becomes

$$
\begin{aligned}
&H^{\Gamma_6} = H_c + H_f + H^{\Gamma_6}_{\rm hyb},\\
&H_c = \sum_{\boldsymbol{k}}\sum_{\sigma}\left(\varepsilon^c_{\boldsymbol{k}} - \mu_c\right)c^\dagger_{\boldsymbol{k}\sigma}c_{\boldsymbol{k}\sigma},\\
&H_f = \sum_{i}\sum_{\tau}(\epsilon_f - \mu_c)f^\dagger_{i\tau}f_{i\tau} + U\sum_i n_{fi\tau}n_{fi-\tau},\\
&H^{\Gamma_6}_{\rm hyb} = \sum_{\boldsymbol{k}}[c^\dagger_{\boldsymbol{k}\uparrow}\quad c^\dagger_{\boldsymbol{k}\downarrow}]\boldsymbol{d}_{\Gamma_6}(\boldsymbol{k})\cdot\hat{\boldsymbol{\sigma}}\begin{bmatrix}f_{\boldsymbol{k}+}\\ f_{\boldsymbol{k}-}\end{bmatrix} + \text{H.c.},
\end{aligned}
$$

with

$$
\begin{aligned}
&\varepsilon_f = \varepsilon_{f\Gamma_6},\\
&\boldsymbol{d}_{\Gamma_6}(\boldsymbol{k}) = (-2\mathrm{i}V_{sf}\sin k_x, 2\mathrm{i}V_{sf}\sin k_y, 4\mathrm{i}V'_{sf}\sin k_z),\\
&f_{\boldsymbol{k}\tau} = f_{\boldsymbol{k}\Gamma_6\tau},
\end{aligned}
$$

where V'_{sf} corresponding to the hybridization to the z direction is modified by the tetragonal surroundings. Here, $\varepsilon^c_{\boldsymbol{k}}$ is the dispersion relation of conduction electrons in the tetragonal surroundings.

APPENDIX B: REVIEW OF THE Z_2 TOPOLOGICAL INDEX

We review the parity eigenvalue in the Z_2 topological indices of Eqs. (26) and (27). Generally speaking, any four-by-four matrices with the Hermitian property can be decomposed by the identity matrix $\boldsymbol{I}$, five Dirac matrices $\boldsymbol{\Gamma}^a$, and their ten commutators $\boldsymbol{\Gamma}^{ab} = [\boldsymbol{\Gamma}^a, \boldsymbol{\Gamma}^b]/(2\mathrm{i})$. Thus, our Hamiltonian matrix $H^\Gamma(\boldsymbol{k})$ can be expressed in terms of these 16 basis matrices. It is convenient to choose the following representation for the Dirac matrices:

$$
\boldsymbol{\Gamma}^{(1,2,3,4,5)} = (\boldsymbol{\tau}_z\otimes\boldsymbol{\sigma}_0, \boldsymbol{\tau}_x\otimes\boldsymbol{\sigma}_0, \boldsymbol{\tau}_y\otimes\boldsymbol{\sigma}_x, \boldsymbol{\tau}_y\otimes\boldsymbol{\sigma}_y, \boldsymbol{\tau}_y\otimes\boldsymbol{\sigma}_z),
$$

where $\boldsymbol{\tau}_\alpha$ and $\boldsymbol{\sigma}_\alpha$ are 2×2 matrices in the orbital (s and f) and spin spaces, respectively.

An essential aspect is that this general expansion can be simplified near gap closing momentum points, which occur at time-reversal-invariant momentum points $\boldsymbol{k}^*_m$, where the gap closes linearly in momentum, thus the effective theory is given by the Dirac theory. Such a Dirac theory, referred as the Bernevig-Hughes-Zhang model,[35] can be expanded by only $\boldsymbol{I}$ and $\boldsymbol{\Gamma}^a$ as

$$
H^\Gamma_{\boldsymbol{k}^*_m}(\boldsymbol{k}) = d^\Gamma_0(\boldsymbol{k})\boldsymbol{I} + \sum_{a=1}^{5}\boldsymbol{d}^\Gamma_a(\boldsymbol{k})\boldsymbol{\Gamma}^a.
$$

Among these Dirac matrices, $\boldsymbol{\Gamma}^1$ is merely the parity operator $\hat{\boldsymbol{P}}$ in the present representation,

$$
\hat{\boldsymbol{P}} = \boldsymbol{\tau}_z\otimes\boldsymbol{\sigma}_0,
$$

where $\boldsymbol{\tau}_z = +$ and $\boldsymbol{\tau}_z = -$ correspond to s and f orbitals, respectively. The following relations on parity should be noted:

$$
\begin{aligned}
\hat{\boldsymbol{P}}\boldsymbol{\Gamma}^a\hat{\boldsymbol{P}}^{-1} &= \boldsymbol{\Gamma}^a \quad \text{for} \quad a = 1,\\
\hat{\boldsymbol{P}}\boldsymbol{\Gamma}^a\hat{\boldsymbol{P}}^{-1} &= -\boldsymbol{\Gamma}^a \quad \text{for} \quad a \neq 1.
\end{aligned}
$$

Therefore, $\boldsymbol{\Gamma}^1$ is only a parity-even Dirac operator.

For the three-dimensional system, there are eight time-reversal-invariant points $\boldsymbol{k}^*_m$ in the first Brillouin zone. We obtain two invariants at such time-reversal-invariant points, given by

$$
\begin{aligned}
\boldsymbol{\Theta}H^\Gamma(\boldsymbol{k}^*_m)\boldsymbol{\Theta}^{-1} &= H^\Gamma(\boldsymbol{k}^*_m),\\
\hat{\boldsymbol{P}}H^\Gamma(\boldsymbol{k}^*_m)\hat{\boldsymbol{P}}^{-1} &= H^\Gamma(\boldsymbol{k}^*_m),
\end{aligned}
$$

where $\boldsymbol{\Theta}$ is the time-reversal operator. Considering the relation of Dirac matrices on parity transformation, we can easily estimate the eigenvalue at $\boldsymbol{k}^*_m$,

$$
E^\Gamma(\boldsymbol{k}^*_m) = d^\Gamma_0(\boldsymbol{k}^*_m)\boldsymbol{I} + d^\Gamma_1(\boldsymbol{k}^*_m)\hat{\boldsymbol{P}},
$$

where $d^\Gamma_1(\boldsymbol{k}^*_m)$ is given by

$$
d^\Gamma_1(\boldsymbol{k}^*_m) = \tfrac{1}{2}\left[\varepsilon^c_{\boldsymbol{k}^*_m} + \epsilon t(\boldsymbol{k}^*_m) - \epsilon_f - \lambda\right].
$$

Then, the parity eigenvalue δ_m at $\boldsymbol{k}^*_m$ can expressed as follows:

$$
\delta_m = -\mathrm{sgn}\left[d^\Gamma_1(\boldsymbol{k}^*_m)\right] = -\mathrm{sgn}\left[\varepsilon^c_{\boldsymbol{k}^*_m} + \epsilon t(\boldsymbol{k}^*_m) - \epsilon_f - \lambda\right].
$$

APPENDIX C: AN EFFECTIVE DIRAC THEORY FOR THE HYBRIDIZATION COUPLING WITH THE SYMMETRY $\Gamma_{8(2)}$

In the hybridization with $\Gamma_{8(2)}$, the effective Hamiltonian is

$$H(\boldsymbol{k}) = \begin{pmatrix} \varepsilon^c_{\boldsymbol{k}} - \mu_c & Vb(-2i\sin k_x + 2\sin k_y) & 0 & 4Vbi\sin k_z \\ Vb(2i\sin k_x + 2\sin k_y) & -\epsilon t(\boldsymbol{k}) + \widetilde{\epsilon}_f - \mu_c & 4Vbi\sin k_z & 0 \\ 0 & -4Vbi\sin k_z & \varepsilon^c_{\boldsymbol{k}} - \mu_c & -Vb(2i\sin k_x + 2\sin k_y) \\ -4Vbi\sin k_z & 0 & -Vb(-2i\sin k_x + 2\sin k_y) & -\epsilon t(\boldsymbol{k}) + \widetilde{\epsilon}_f - \mu_c \end{pmatrix}.$$

Expanding this Hamiltonian around the $\boldsymbol{k}^*_{\pi\pi\pi}$ point, we reach the following expression for the Dirac theory:

$$H(\boldsymbol{p}) = \begin{pmatrix} h(\mathbf{p}) & g(\mathbf{p}) \\ g^*(\mathbf{p}) & h^*(-\mathbf{p}) \end{pmatrix},$$

where

$$\begin{aligned} h(\boldsymbol{p}) &= \varepsilon(\boldsymbol{p})\sigma_0 + \boldsymbol{d}(\boldsymbol{p})\cdot\boldsymbol{\sigma}, \\ g(\boldsymbol{p}) &= -2Aip_z\sigma_x, \\ \varepsilon(\boldsymbol{p}) &= C - D\left(p_x^2 + p_y^2 + p_z^2\right), \\ \boldsymbol{d}(\boldsymbol{p}) &= (Ap_y, -Ap_x, M(\boldsymbol{p})), \end{aligned}$$

$$\begin{aligned} M(\boldsymbol{p}) &= M - B\left(p_x^2 + p_y^2 + p_z^2\right), \\ C &= 3t + \frac{3}{2}\epsilon + \frac{1}{2}\widetilde{\epsilon}_f - \mu_c, \\ D &= \frac{1}{2}\left(t + \frac{\epsilon}{2}\right), \\ A &= 2Vb, \\ B &= \frac{1}{2}\left(t - \frac{\epsilon}{2}\right), \\ M &= 3t - \frac{3}{2}\epsilon - \frac{1}{2}\widetilde{\epsilon}_f. \end{aligned}$$

[1] J. Goldstone and F. Wilczek, Phys. Rev. Lett. **47**, 986 (1981); M. Stone, Phys. Rev. B **31**, 6112 (1985).
[2] G. W. Semenoff, Phys. Rev. Lett. **53**, 2449 (1984); E. Fradkin, E. Dagotto, and D. Boyanovsky, *ibid.* **57**, 2967 (1986).
[3] E. Witten, Phys. Lett. B **117**, 324 (1982).
[4] S. Ryu, C. Mudry, H. Obuse, and A. Furusaki, Phys. Rev. Lett. **99**, 116601 (2007).
[5] W. P. Su, J. R. Schrieffer, and A. J. Heeger, Phys. Rev. Lett. **42**, 1698 (1979).
[6] F. D. M. Haldane, Phys. Rev. Lett. **61**, 2015 (1988).
[7] D. J. Thouless, M. Kohmoto, M. P. Nightingale and M. den Nijs, Phys. Rev. Lett. **49**, 405 (1982).
[8] C. L. Kane and E. J. Mele, Phys. Rev. Lett. **95**, 146802 (2005); **95**, 226801 (2005).
[9] L. Fu, C. L. Kane, and E. J. Mele, Phys. Rev. Lett. **98**, 106803 (2007); L. Fu and C. L. Kane, Phys. Rev. B **76**, 045302 (2007).
[10] J. E. Moore and L. Balents, Phys. Rev. B **75**, 121306 (2007).
[11] R. Roy, Phys. Rev. B **79**, 195322 (2009); **79**, 195321 (2009).
[12] D. Pesin and L. Balents, Nat. Phys. **6**, 376 (2010).
[13] L. Balents, Nature (London) **464**, 199 (2010).
[14] R. Moessner and S. L. Sondhi, Phys. Rev. Lett. **86**, 1881 (2001); R. Moessner, S. L. Sondhi, and E. Fradkin, Phys. Rev. B **65**, 024504 (2001); K. S. Raman, R. Moessner, and S. L. Sondhi, Phys. Rev. B **72**, 064413 (2005).
[15] Z. Y. Meng, T. C. Lang, S. Wessel, F. F. Assaad, and A. Muramatsu, Nature (London) **464**, 847 (2010); B. K. Clark, D. A. Abanin, and S. L. Sondhi, Phys. Rev. Lett. **107**, 087204 (2011).
[16] O. Sikora, F. Pollmann, N. Shannon, K. Penc, and P. Fulde, Phys. Rev. Lett. **103**, 247001 (2009); F. Pollmann, J. J. Betouras, K. Shtengel, and P. Fulde, *ibid.* **97**, 170407 (2006).
[17] A. Kitaev, Ann. Phys. (NY) **321**, 2 (2006).
[18] N. Read and D. Green, Phys. Rev. B **61**, 10267 (2000).
[19] T. Senthil, A. Vishwanath, L. Balents, S. Sachdev, and M. P. A. Fisher, Science **303**, 1490 (2004); T. Senthil, L. Balents, S. Sachdev, A. Vishwanath, and M. P. A. Fisher, Phys. Rev. B **70**, 144407 (2004).
[20] A. W. Sandvik, Phys. Rev. Lett. **104**, 177201 (2010); **98**, 227202 (2007).
[21] G. Chen, J. Gukelberger, S. Trebst, F. Alet, and L. Balents, Phys. Rev. B **80**, 045112 (2009).
[22] T. Neupert, L. Santos, C. Chamon, and C. Mudry, Phys. Rev. Lett. **106**, 236804 (2011); E. Tang, J.-W. Mei, and X.-Gang Wen, *ibid.* **106**, 236802 (2011); K. Sun, Z. Gu, H. Katsura, and S. Das Sarma, *ibid.* **106**, 236803 (2011).
[23] J. Maciejko, X.-L. Qi, A. Karch, and S.-C. Zhang, Phys. Rev. Lett. **105**, 246809 (2010).
[24] K.-S. Park and H. Han, Phys. Rev. B **82**, 153101 (2010).
[25] B. Swingle, M. Barkeshli, J. McGreevy, and T. Senthil, Phys. Rev. B **83**, 195139 (2011).
[26] M. Hohenadler, T. C. Lang, and F. F. Assaad, Phys. Rev. Lett. **106**, 100403 (2011).
[27] S. Rachel and K. Le Hur, Phys. Rev. B **82**, 075106 (2010); J. He, Y.-H. Zong, S.-P. Kou, Y. Liang, and S. Feng, *ibid.* **84**, 035127 (2011); M. W. Young, S.-S. Lee, and C. Kallin, *ibid.* **78**, 125316 (2008).
[28] M. Dzero, K. Sun, V. Galitski, and P. Coleman, Phys. Rev. Lett. **104**, 106408 (2010); M. Dzero, K. Sun, P. Coleman, and V. Galitski, Phys. Rev. B **85**, 045130 (2012).
[29] H. v. Lohneysen, A. Rosch, M. Vojta, and P. Wolfle, Rev. Mod. Phys. **79**, 1015 (2007); P. Gegenwart, Q. Si, and F. Steglich, Nat. Phys. **4**, 186 (2008).
[30] K. Takegahara, Y. Aoki, and A. Yanase, J. Phys. C **13**, 583 (1980).
[31] T. Senthil, S. Sachdev, and M. Vojta, Phys. Rev. Lett. **90**, 216403 (2003); T. Senthil, M. Vojta, and S. Sachdev, Phys. Rev. B **69**, 035111 (2004).

[32]C. Pepin, Phys. Rev. Lett. **98**, 206401 (2007); Phys. Rev. B **77**, 245129 (2008).

[33]The form factor in the hybridization term can be expressed as follows:

$$[\boldsymbol{d}_\Gamma(\boldsymbol{k})\cdot\hat{\boldsymbol{\sigma}}]_{\sigma\alpha}=\sqrt{4\pi}\sum_{j_z=-j}^{j}b_{j_z}^{\alpha}\sum_{m}a_{lm\sigma}^{j_z}Y_l^m(\Omega_{\boldsymbol{k}}),$$

where $a_{lm\sigma}^{j_z}$ is the Clebsh-Gordan coefficient, b_{j_z} is a coefficient specifying the crystal level, and $Y_l^m(\Omega_{\boldsymbol{k}})$ is the spherical harmonic function.

[34]T. Senthil and P. A. Lee, Phys. Rev. B **79**, 245116 (2009); Phys. Rev. Lett. **103**, 076402 (2009).

[35]B. A. Bernevig, T. L. Hughes, and S. C. Zhang, Science **314**, 1757 (2006); M. Konig, S. Wiedmann, C. Brune, A. Roth, H. Buhmann, L. W. Molenkamp, X. L. Qi, and S. C. Zhang, *ibid.* **318**, 766 (2007).

[36]K.-S. Kim and C. Jia, Phys. Rev. Lett. **104**, 156403 (2010).

[37]I. Martin and C. D. Batista, Phys. Rev. Lett. **101**, 156402 (2008); Y. Kato, I. Martin, and C. D. Batista, *ibid.* **105**, 266405 (2010); S. Kumar and J. van den Brink, *ibid.* **105**, 216405 (2010); G.-W. Chern, *ibid.* **105**, 226403 (2010).

[38]K.-S. Kim and T. Takimoto, Phys. Rev. B **83**, 245138 (2011).

[39]S. Florens and A. Georges, Phys. Rev. B **66**, 165111 (2002); **70**, 035114 (2004).

[40]K.-S. Kim, Phys. Rev. Lett. **97**, 136402 (2006).

[41]M.-T. Tran and K.-S. Kim, Phys. Rev. B **83**, 125416 (2011); K.-S. Kim and M. D. Kim, *ibid.* **81**, 075121 (2010).

[42]T. Takimoto, J. Phys. Soc. Jpn. **80**, 123710 (2011).

[43]The metallic in-gap states appear only in the temperature region lower than the hybridization gap, above which SmB_6 behaves like a typical insulator.